Experiments and simulations on Al-Au mixtures and mixtures laws

Jean Clérouin,* Vanina Recoules, Stéphane Mazevet, Pierre Noiret, and Patrick Renaudin
Département de Physique Théorique et Appliquée, CEA/DAM Île-de-France Boîte Postale 12, 91680 Bruyères-le-Châtel Cedex, France
(Received 27 February 2007; published 22 August 2007)

We measured the thermodynamical and transport properties of aluminum-gold mixtures in the warm dense matter regime and for various concentrations. We compare these measurements with quantum molecular dynamics (QMD) simulations. We find that the calculated pressures and resistivities of both the mixtures and pure phases are in good agreement with the measurements. This further allows us to test the mixing rules usually employed to predict the properties of the mixed phases from the pure ones. We show, in this regime, that the partial densities mixing rule predicts the pressure of the mixture rather accurately but fails in its prediction of the optical conductivity. To improve this latter prediction, we find that we must invoke an isothermal-isobaric mixture rule to compute the pure phase contributions at the correct densities.

DOI: 10.1103/PhysRevB.76.064204 PACS number(s): 52.25.−b, 52.65.−y, 52.50.−b, 52.70.−m

I. INTRODUCTION

Our understanding of matter at the thermodynamical conditions encountered in some astrophysical objects or in laser fusion experiments relies on our ability to describe the properties of mixtures properly. Giant planets are made of a mixture of hydrogen and helium (with traces of other elements),[1,2] the interior of the Sun is a mixture of iron and hydrogen,[3] and inertial confinement fusion pellets are always subjected to the mixing of the different layers constituting the envelope (beryllium, CH plastics, deuterium, gold, etc.) during the compression process.[4] In the latter case, we are interested here by the warm dense matter regime (WDM) which is characterized by a strong coupling and a high electronic degeneracy. This regime is rather difficult to describe for pure phases but becomes even more challenging for mixtures. When using hydrocodes to model such systems, one needs to know the thermodynamical properties of the system from the tabulated values of pure phases, following some given mixing rule. There are different mixing rules in use, starting from the simplest, the partial densities mixing rule (PDMR), to more complex ones such as the isothermal-isobaric mixing rule (IIMR) or isoelectronic mixing rule (IEMR). These mixing rules have their own range of validity but have only been scarcely tested in the WDM regime.[5] Our purpose in this paper is to provide experimental data on aluminum-gold mixtures with varying concentration, and to test this conventionally used mixing rule using both these data and quantum molecular dynamics simulations. Aluminum and gold were chosen because the pure phases have been previously studied in detail both numerically and experimentally.[6–9]

Starting our numerical work from a pure aluminum phase ($M0$) at a density of 0.1 g/cm^3 (16 atoms in a box of 19.08 Å), we substituted an increasing number of aluminum atoms by gold atoms while keeping the total number of atoms constant and until we reach the pure gold phase ($M5$). For the mixture $M1$, we used 32 atoms in a box of 24.04 Å. For the pure phase of gold ($M5$), we increased the size of the box up to 21.08 Å to comply with the experimental limitations. This leads to a density of 0.5 g/cm^3 instead of 0.76 g/cm^3. The composition of intermediate mixtures ($M1$ to $M4$) are presented in Table I. ($M1$) is aluminum rich (96.8% aluminum) while ($M4$) is gold rich (62.5% gold). ($M2$) and ($M3$) are rich in number of aluminum atoms but not in mass. Except for the ($M2$) mixture for which no experiment was performed, all compositions have been studied both experimentally and theoretically.

The partial density of each species $i=1,2$ made of N_i atoms in a box of side a is given by $\rho_i=\frac{N_iA_i}{a^3\mathcal{N}}$, where $\mathcal{N}$ is the Avogadro number. Using the total number $N=N_1+N_2$, we define the atomic fractions by $x_1=N_1/N$ and $x_2=N_2/N$ and the mass concentrations by

$$c_1=\frac{x_1A_1}{\bar{A}} \quad \text{and} \quad c_2=\frac{x_2A_2}{\bar{A}},$$

where $\bar{A}$ is the average mass given by

$$\bar{A}=x_1A_1+x_2A_2. \tag{1}$$

II. EXPERIMENTS

The experimental measurements were performed in the "Enceinte à Plasma Isochore" (EPI) described in previous papers.[7,10] We just recall here that the EPI combines two existing techniques: a high-pulse power-bank to obtain a fast heating of the metallic sample and a high-pressure closed-

TABLE I. Properties of studied mixtures. The box is larger for $M5$ to comply with the experimental limitations.

	N_{tot}	N_{Al}	N_{Au}	x_{Al}	x_{Au}	$\bar{A}$ g	ρ_{Al} g/cm^3	ρ_{Au} g/cm^3	ρ_{tot} g/cm^3
$M0$	16	16	0	1	0	27	0.1	0	0.1
$M1$	32	31	1	0.968	0.031	32.24	0.1	0.024	0.124
$M2$	16	13	3	0.812	0.187	58.86	0.084	0.141	0.225
$M3$	16	10	6	0.625	0.375	90.75	0.064	0.283	0.348
$M4$	16	6	10	0.375	0.625	133.25	0.039	0.471	0.510
$M5$	16	0	16	0.0	1	197	0	0.5	0.5

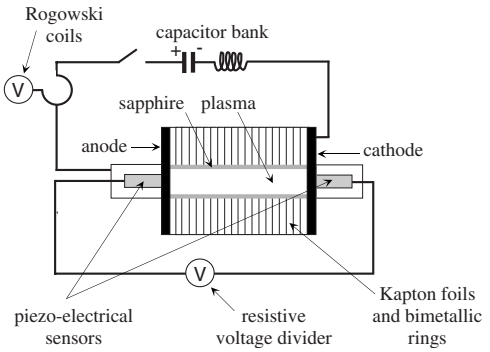

FIG. 1. Experimental configuration of the EPI device.

vessel sketched in Fig. 1. The body of the vessel consists in an alternate stack of autofrettaged bimetallic rings (1 cm thickness) and electrical insulator Kapton foils (125 μm) leading to a volume of the inner plasma channel of 20 cm^3. There is no particular difficulty in setting up mixture experiments. Proper quantities of each component of the mixture are introduced in the vessel, following the partial densities given in Table I. For this mixture we used a bundle of mixed wires cut at the proper length. The input energy is adjusted to comply with the pressure limit of the vessel. Energies, pressures, and conductivities are measured in an absolute way and the interpretation does not need any external model. The temperature is not measured and to be consistent our results are presented versus the internal energy. For each shot, the input energy and the plasma resistance $R(t)$ are inferred from the current and voltage measurements. The resistivity κ of the plasma is determined by using the relation $\kappa(t) = \pi r^2 R(t)/l$, where l and r are, respectively, the length and the radius of the plasma channel, determined by the geometry of the vessel. The uncertainty in the current and voltage measurements produces a 15% uncertainty in the resistance of the plasma. The internal energy variation δU can be evaluated from the electrical energy input E_{el} and is given by $\delta U = (E_{\mathrm{el}} - E_{\mathrm{rad}}) + \delta W$, where E_{rad} is the thermal loss at the vessel walls. The mechanical work loss δW due to the vessel expansion under pressure is less than 1% of E_{el} and can be neglected. The thermal losses are assumed to be radiative during the plasma phase, and negligible before. Radiative losses of a blackbody of surface S are given by $dE_{\mathrm{rad}}/dt = \sigma \times S \times T^4$, where σ is the Stefan-Boltzmann constant. Piezoelectric measurements of the pressure at each end of the plasma channel are also leading to an uncertainty of 15%.

III. SIMULATIONS

In the thermodynamical regime of interest ($\rho \simeq \rho_0/10$ and 5000 K $< T <$ 40 000 K), quantum molecular dynamics (QMD) simulations have shown to be an efficient tool to predict simultaneously both thermodynamics properties and transport properties. Despite some well known limitations at high temperatures (beyond 5 eV) resulting from the use of pseudopotentials and the number of states that can be included, the QMD method is particularly suited to describe various situations in the WDM regime. The method is by construction particularly adapted to mixtures without any further assumptions in contrast to average atom models[11] which are limited to the description of pure phases.

The simulations were performed using PAW pseudopotentials[12] with the electronic structure package VASP developed at the University of Vienna.[13] For aluminum, the pseudopotential used three active electrons ($3s^2 3p^1$) with a cutoff energy of 240 eV. 11 electrons are included in the Au pseudopotential ($5d^{10} 6s^1$) with an energy cutoff of 229 eV. The exchange and correlation terms were treated at the level of the LDA approximation[14] and using the Ceperley-Alder parametrization.[15] During the molecular dynamics simulations, the Brillouin zone was sampled at the Γ point, whereas we used more refined k-point sampling such as 2^3 and 3^3 in the Monkhorst-Pack scheme, for the optical calculations. The ionic trajectories were generated for 16 atoms of mixture during 1000 time steps of 0.2 fs after equilibration. The mixture simulations were performed in the microcanonical ensemble, at constant total energies, as well as the isokinetic ensemble for the simulations at partial densities in order to ensure an easier control of the temperatures. For each temperature, the initial conditions were taken from a previous simulation performed at lower temperature to speed up the equilibration time. We assume that we reach equilibrium when records of pressures versus time are showing a steady average and enough oscillations around the average value (5 to 10 oscillations). We also tested the convergency of the simulations with the number of atoms by running 4, 16, and 32 ions simulations, without noticeable changes. The fact that at high temperature and low density the system can be accurately simulated by a small number of ions was already pointed by Desjarlais for simulation of aluminum at very low density and high temperature.[6]

From the knowledge of the Kohn-Sham orbitals ψ_n, energies ϵ_n, and occupations f_n, the conductivity was computed using the Kubo-Greenwood formulation on selected ionic configurations

$$\sigma(\omega) = \frac{2\pi}{3\omega}\frac{1}{\Omega}\sum_{n,m,\alpha}\sum_{\boldsymbol{k}} W(\boldsymbol{k})(f_n - f_m) \times |\langle \psi_n^{\boldsymbol{k}} | \nabla_\alpha | \psi_m^{\boldsymbol{k}} \rangle|^2 \delta(\epsilon_m^{\boldsymbol{k}} - \epsilon_n^{\boldsymbol{k}} - \hbar\omega), \tag{2}$$

where $\boldsymbol{k}$ and $W(\boldsymbol{k})$ are the vectors and the weight in the Brillouin zone, $\boldsymbol{\nabla}_\alpha$ is the velocity operator in each direction ($\alpha = x, y, z$) between two states n and m with occupation f_n and f_m. The dc conductivity is obtained by taking the zero frequency limit of $\sigma(\omega)$. Optical properties are obtained[16] from the computation of the imaginary part of the conductivity σ_2 given by the Kramer-Krönig relations

$$\sigma_2(\omega) = -\frac{2}{\pi} P \int \frac{\sigma(\nu)\nu}{(\nu^2 - \omega^2)} d\nu, \tag{3}$$

where P stands for the principal value of the integral. From the complex conductivity, we get the real and imaginary part of the dielectric function

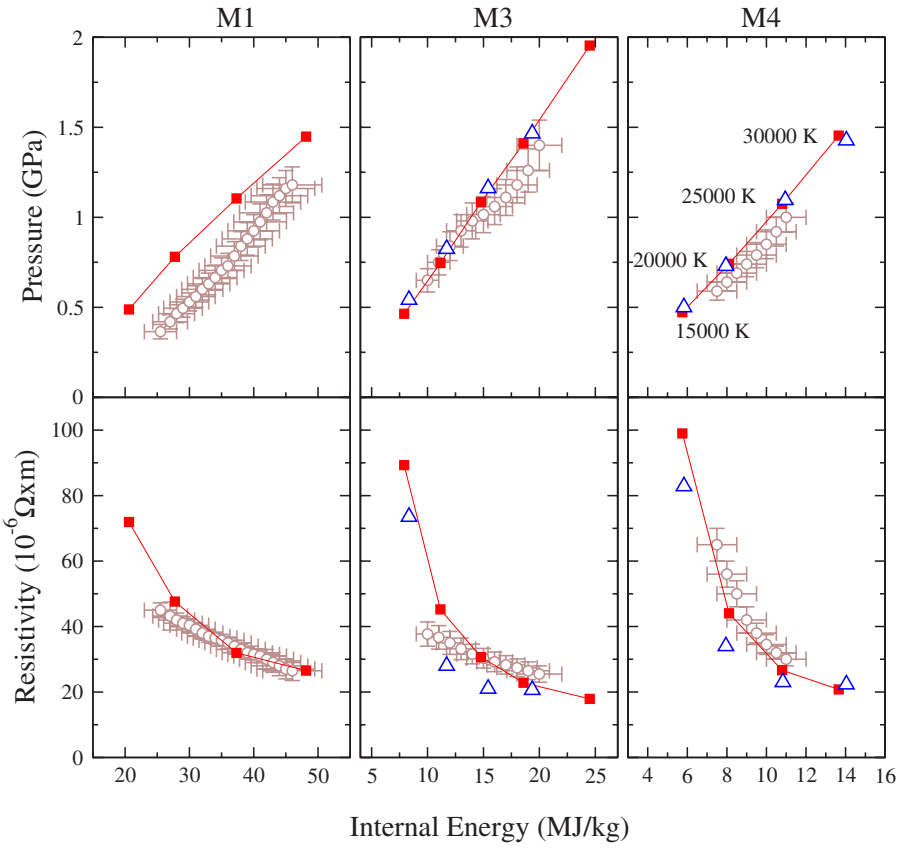

FIG. 2. (Color online) Pressures (top) and resistivities (bottom) versus energy for the three mixtures $M1$, $M3$, and $M4$ as given in Table I. Gray circles with errors bars: experimental data, red squares: QMD simulations of the mixtures. The red line is to guide the eyes. The blue triangles are the composition of QMD simulations performed at partial densities (PDMR) as given in Table I.

$$\epsilon_1(\omega) = 1 - \frac{4\pi}{\omega}\sigma_2(\omega) \quad \text{and} \quad \epsilon_2(\omega) = \frac{4\pi}{\omega}\sigma(\omega). \tag{4}$$

This dielectric function leads to indexes given by $\epsilon = n^2$,

$$\epsilon(\omega) = \epsilon_1 + i\epsilon_2 = [n(\omega) + ik(\omega)]^2, \tag{5}$$

from which the reflectivity $r(\omega)$ and the absorption coefficient $\alpha(\omega)$ are computed,

$$r(\omega) = \frac{[1-n(\omega)]^2 + k^2(\omega)}{[1+n(\omega)]^2 + k^2(\omega)} \quad \text{and} \quad \alpha = \frac{4\pi}{n(\omega)c}\sigma(\omega). \tag{6}$$

IV. RESULTS

A. Direct simulations of mixture

For each composition ($M1$, $M3$, and $M4$), we performed a direct QMD simulation of the mixture using the atom numbers given in Table I and at four different temperatures (15 000, 20 000, 25 000, and 30 000 K). By comparing the total energy obtained with the one resulting from the mixing of the energies of the solid phases at 300 K ($E = c_1E_1 + c_2E_2$), we obtain the reference energy for each mixture. This allows a direct comparison with the experimental measurement as shown in Fig. 2. For each composition, we can see that the pressures (Fig. 2, top panel) obtained by QMD are in good agreement with the experimental results except for the mixture $M1$ (3.2% Au by number) for which the agreement is less satisfactory. For the resistivities (Fig. 2, bottom panel), we have a good agreement in all cases. We point out that these results recover the now well known property of warm expanded metals where the resistivity decreases with temperature and hence with the energy.[17,18] QMD simulations outside the experimental domain are showing a dramatic increase of the resistivity at low energy. This is a low temperature metal-to-insulator transition.

B. Equation of state of pure elements

To test mixture rules, one must first rely on the equations of state (EOS) for the pure phases. As shown in Fig. 3, we have for aluminum a very good agreement between the experimental data and the EOS computed by Bushman, Lomonosov, and Fortov (BLF).[19] We point out that the QMD simulations are closer to the SESAME No. 3719 (Ref. 20) which overestimates significantly the experimental data. This difference explains the disagreement observed in Fig. 2 for the aluminum rich mixture $M1$. We also find that this discrepancy increases with the energy (or with the temperature). While this may indicate a shortcoming of the DFT at describing this element in this regime, we do not completely rule out, however, some imperfections in the pressure measurements for this particular data set.

For gold, we find a very good agreement between the experimental data, the QMD simulations, and the SESAME EOS No. 2710, as shown in Fig. 4. It must be stressed that, for gold, the previous SESAME EOS No. 2700 as well as the QEOS model[21] were both overestimating the experimental and QMD pressures in this regime. For gold, we also find that the BLF EOS strongly underestimates the experimental pressures.

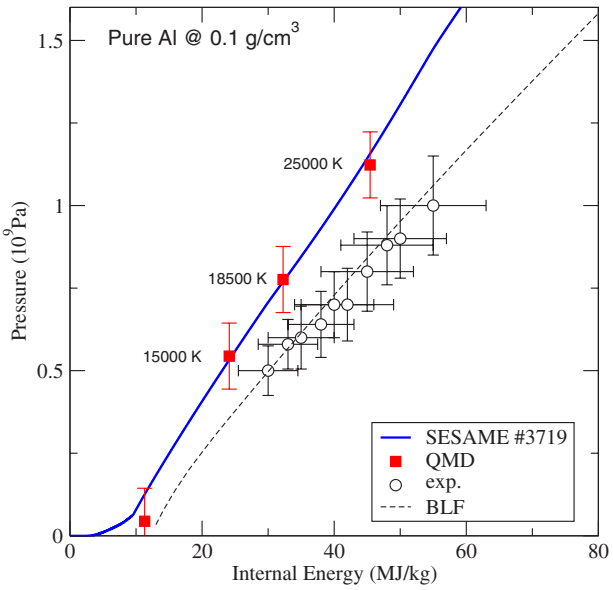

FIG. 3. (Color online) Aluminum equation of state at 0.1 g/cm^3. Experimental data (circles) are compared with SESAME No. 2719 (thick line), BLF EOS (dashed line), and QMD (squares). QMD temperatures are also indicated.

We have built a linear fit, accurate in the range of densities and temperatures investigated here, to facilitate the use of the QMD results in a mixture model. These linear fits are in the form

$$P(\mathrm{GPa}) = a + b \times \rho(\mathrm{g/cm^3}), \tag{7}$$

where the coefficients are given in Table II. In Fig. 5, we show the variation of pressure as a function of volume for aluminum and gold. V_i is the partial volume, $V_i = x_i A_i / \rho$, for each species concentrations as given in Table I. To facilitate the graphical interpretation, we also plot the symmetric line $V_{\mathrm{Al}} \rightarrow -V_{\mathrm{Al}}$ on the volume axis for aluminum.

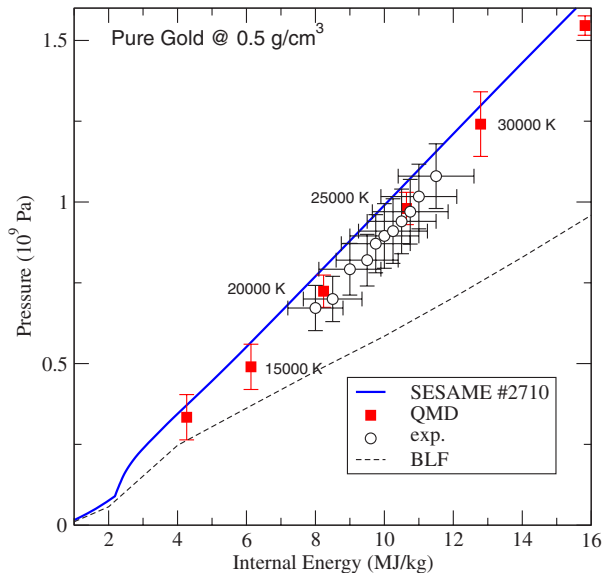

FIG. 4. (Color online) Gold equation of state at 0.5 g/cm^3. Experimental data (circles) are compared with SESAME No. 2710 (thick line), QMD (squares), and BLF (dashed line). Temperatures of the QMD simulations are indicated.

TABLE II. Linear fits coefficients [Eq. (7)] for the Al and Au isotherms.

	T (K)	a	b
Al	15 000	−0.001	0.543
	20 000	−0.001	7.954
	25 000	−0.068	11.94
	30 000	−0.074	15.0
Au	15 000	0.044	0.527
	20 000	0.034	0.927
	25 000	0.078	1.324
	30 000	0.048	1.851

C. Mixture rules

The question is now how to predict mixtures properties from the pure elements ones. The determination of the thermodynamical conditions of the pure phases, and the way to combine the associated properties, are known as mixture rules. The simplest one is the partial densities mixing rule (PDMR), which directly results from the ideal gas law. For this first rule, the components of the mixture are filling the entire volume V and the total pressure is given by the sum of the partial pressures

$$\text{Partial densities} \begin{cases} P = P_1 + P_2, \\ V = V_1 = V_2, \\ E = c_1 E_1 + c_2 E_2. \end{cases} \tag{8}$$

A second approach was proposed by More to mix the equation of state in the framework of the QEOS model.[21] In this model, known as the isothermal-isobaric mixing rule (IIMR), each component of the mixtures occupies a volume V_α. The volume V_α is adjusted until the partial pressures are equal and this under the constrain of total volume conservation

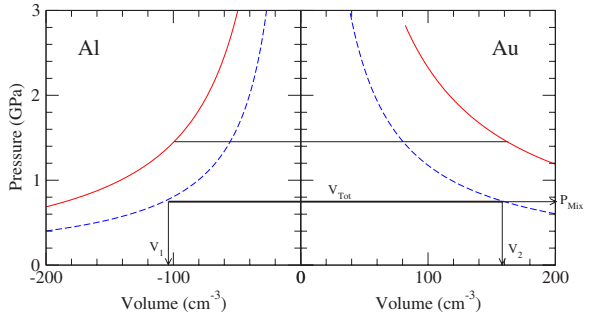

FIG. 5. (Color online) Left: Pressure vs volume for aluminum along two isotherms 20 000 K (dashed line) and 30 000 K (full line). Right: same for gold. The heavy horizontal line shows the total volume of the mixture and the partial volumes are indicated by arrows.

$$\text{Isothermal-isobaric} \begin{cases} P = P_1 = P_2, \\ V = V_1 + V_2, \\ E = c_1 E_1 + c_2 E_2. \end{cases} \quad (9)$$

We can thus define a volume fraction $\alpha_i = V_i / V_{\text{tot}}$ for each species.

A third approach, based on the equality of the electronic densities, is referred to the iso-electronic mixing rule (IEMR). In this case, the partial volumes are adjusted in order to get the equality of the electronic densities at a given total volume. Practically, this approach rest on an ionization model, such as the More ionization models,[22] to predict the ionization state at a given thermodynamical condition. Unfortunately, ionization models based on Thomas-Fermi description are strongly overestimating the ionization state in the expanded regime. In this situation, a perfect gas estimation of the ionization is usually preferred and is expressed as

$$PV = (1 + Z^*)NkT. \quad (10)$$

By comparing Eq. (10) with Figs. 3 and 4, we can compute an average ionization for each species. For aluminum, we obtain $Z^* = 0.27$ and 0.54 at a temperature of, respectively, 20 000 and 30 000 K. For gold, we have $Z^* = 0.15$ and 0.53 for the corresponding temperatures.

Mixture rules can be also used to predict the conductivity spectra and the absorption spectra. Mixing conductivities is highly nontrivial and depends on the conductivities of each species as well as on their spatial arrangement. We can express the conductivity of the mixture in a "parallel" formulation

$$\sigma_{\text{mix}} = \alpha_1 \sigma_1 + \alpha_2 \sigma_2, \quad (11)$$

where α_i are the volume fraction for each species. One can also invoke a "serial" formulation for the resistivities κ

$$\kappa_{\text{mix}} = \alpha_1 \kappa_1 + \alpha_2 \kappa_2. \quad (12)$$

A more sophisticated model has also been proposed by Landauer[23] and used by Shepherd[5] to interpret conductivity experiments of strongly correlated plasmas of C_2H_3. In this model, the conductivity of the mixture is given

$$\sigma_{\text{mix}} = \frac{1}{4}((3\alpha_2 - 1)\sigma_2 + (3\alpha_1 - 1)\sigma_1 + \{[(3\alpha_2 - 1)\sigma_2 + (3\alpha_1 - 1)\sigma_1]^2 + 8\sigma_1\sigma_2\}^{1/4}). \quad (13)$$

For microscopically homogeneous plasmas and similar conductivity values, we found that the two formulations (11) and (13) of the mixture properties are leading to similar results. This is also the case for the "serial" only if a volume fraction can be defined as it is the case in the IIMR formulation. With the PDMR, each phase fills the whole volume. This leads to a volume fraction equal to 1 and to a simple addition rule. In this case, formulations (11) and (12) are giving a significantly different estimation. We believe that the "serial" law is not valid for microscopic mixtures. For the sake of simplicity we will take the formulation (11) extended at finite frequency, to obtain the conductivities of the mixture

$$\sigma_{\text{mix}}(\omega) = \alpha_1 \sigma_1(\omega) + \alpha_2 \sigma_2(\omega). \quad (14)$$

D. Partial pressure mixing

To test the PDMR, we performed simulations for mixtures $M4$ and $M3$ for each pure phase at the partial densities given in Table I and for temperatures of 15 000, 20 000, 25 000, and 30 000 K. As shown in Fig. 2 the PDMR yields an estimation of the total pressure (triangle) in excellent agreement with the results of the direct simulation of the mixture. These pressures can also be predicted using the fit (7). For the $M4$ mixture at a temperature of 20 000 K, we obtain a pressure

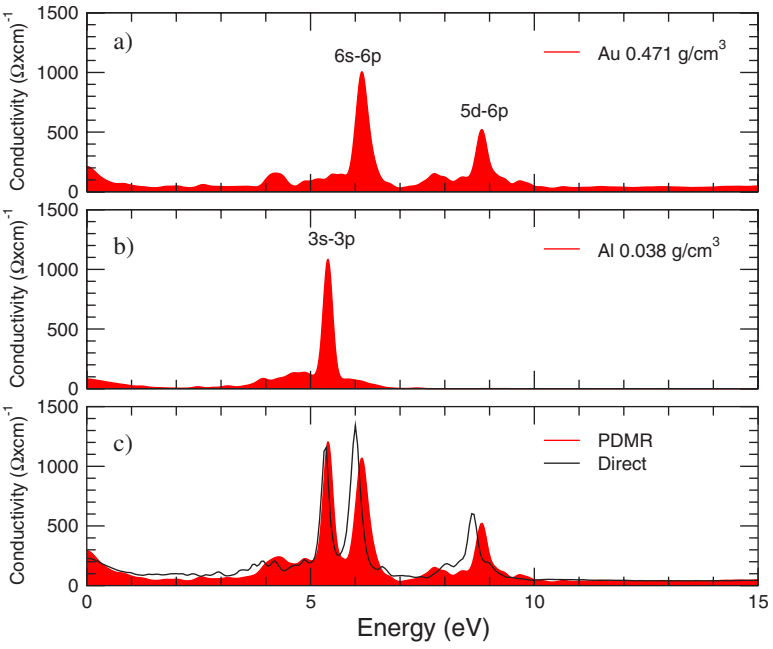

FIG. 6. (Color online) Calculated conductivity spectra for the pure Au (a) and Al (b) phases at 20 000 K for the $M4$ mixture partial densities and (c) comparison of the direct simulation results for the mixture (black line) with the results obtained using the PDMR mixing rule (red surface).

TABLE III. Densities and volumic fractions determined with the IIMR for species 1 and 2 (aluminum and gold), for mixture $M4$ and various temperatures. P_{mix} is the pressure after solving Eq. (9).

T K	P_{mix} GPa	ρ_1 g/cm^3	ρ_2 g/cm^3	α_1	α_2
15 000	0.48	0.089	0.832	0.435	0.565
20 000	0.76	0.097	0.782	0.399	0.601
25 000	1.11	0.098	0.776	0.394	0.606
30 000	1.45	0.102	0.759	0.380	0.620

of 0.308 GPa for aluminum and 0.471 GPa for gold at the partial densities of, respectively, $\rho_1=0.039$ g/cm^3 and $\rho_2=0.471$ g/cm^3 (see Table I). The sum of the partial pressures yields a total pressure of 0.779 GPa for the mixture which is in very good agreement with the direct computation of the pressure (0.742 GPa).

The PDMR formulation (11) leads to a simple addition rule for the conductivity

$$\sigma_{\mathrm{mix}}^{\mathrm{dc}} = \sigma_1^{\mathrm{dc}} + \sigma_2^{\mathrm{dc}}. \tag{15}$$

This expression is consistent with a Drude model where the total conductivity results from the total number of charge carriers, if we assume the same relaxation time. The resistivity of the mixture is compared with the direct calculation of the mixture in the lower panel of Fig. 2 and appears systematically lower than the direct computation, i.e., the conductivity of the mixture is lower than the sum of the conductivities in the PDMR.

Panels (a) and (b) of Fig. 6 show the optical conductivities of the pure phases at partial densities computed for mixture $M4$ at 20 000 K. The interband transitions $3s$-$3p$ for aluminum and $6s$-$6p$, $5d$-$6p$ for gold are clearly identified as well as the Drude behavior at low photon energy. The comparison between the sum of the partial contributions and the direct computation of the mixture, shown in panel (c), brings about two comments. First, as mentioned before, the predicted dc resistivity is much lower than the resistivity of the mixture. Second, the interband transitions for gold are systematically shifted to higher energy. This shift is a density effect which indicates some weakness in the PDMR formulation. In other words, the atoms feel an effective density much higher than the partial density $\rho_i=N_i/V_{\mathrm{tot}}$. This effect is corrected by the isothermal-isobaric mixture law.

E. Isothermal-Isobaric mixing

We now turn to the IIMR, as given by Eq. (9). This leads to a rather different procedure to compute the partial densities. Starting from equal densities, we use the fit (7) to get the partial pressure of each component. By varying the densities, we then search for the combination which leads to the same pressure for both species. The sum of the partial volumes is then compared to the total volume. The partial densities are corrected and the iterative process is restarted until equal pressures and total volume conservation are obtained. This procedure leads to very different partial densities as shown in Table III for the $M4$ mixture. For example, at a temperature of 20 000 K, we get a density of 0.097 g/cm^2 for aluminum instead of 0.0387 g/cm^3 and 0.782 g/cm^3 for

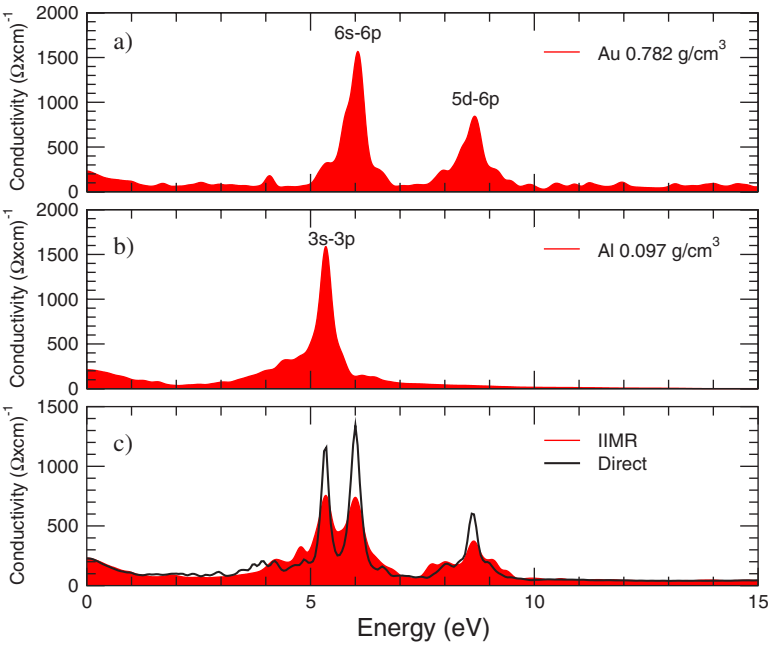

FIG. 7. (Color online) Same as Fig. 2 but with the IIMR. Note the change in the partial densities.

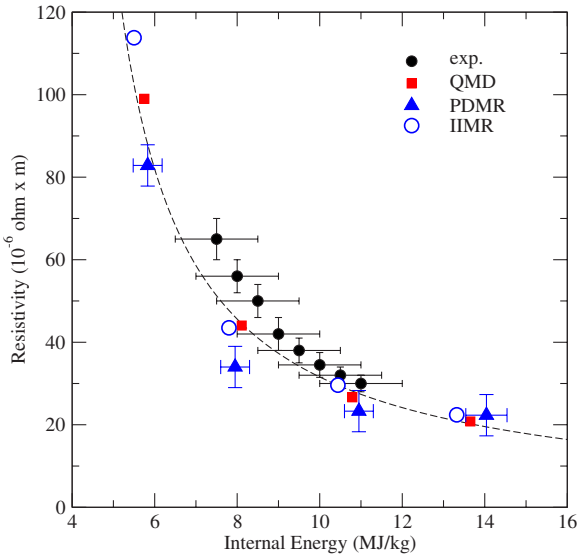

FIG. 8. (Color online) Resistivities versus internal energy. Comparison between PDMR (triangles), IIMR (open circles), direct calculation with QMD (squares), and experimental data (black full circles).

gold instead of 0.471 g/cm^3 for a pressure (equal for each specie) of 0.76 GPa. In contrast with the PDMR model, the partial densities are now depending on temperature.

A graphical interpretation of this process is shown in Fig. 5. In this scheme, the partial volumes are obtained by searching the pressure value at which the horizontal distance between the two corresponding isotherms of aluminum and gold exactly matches the total volume (heavy line in Fig. 5) given by $V_{\mathrm{tot}}=\bar{A}/\rho_{\mathrm{tot}}$. The corresponding volumes and pressure are indicated by arrows. It must be noted that the leading pressure is the result of the IIMR optimization procedure and thus has no reason to coincide with the total pressure of the mixture. Nevertheless, as shown in Table III, the resulting pressures are in close agreement with the direct simulation.

The composition of the optical conductivities follows Eq. (14), with the volume fractions given in Table III. The result is shown in Fig. 7. The features of the pure phases are similar to the one obtained in Fig. 6 with the same atomic transitions but with broader peaks and shifted to lower energies. The composition of the conductivities is now different. The total dc conductivity is closer to the direct result, as shown in Fig. 8. We also note that the atomic transitions are now positioned at the correct energy. In contrast, the intensity of the peaks is reduced.

If we estimate the ionization using Eq. (10), we obtain the electronic density using the partial densities given in Table III. At 20 000 K, we get a density of 5.8×10^{20} cm^{-3} for aluminum and 3.6×10^{20} cm^{-3} for gold. At 30 000 K, we get a density of 1.22×10^{21} cm^{-3} for aluminum and 1.23×10^{21} cm^{-3} for gold. From these results, we conclude that the IIMR is equivalent to the IEMR at high temperature, but fails at low temperature due to a larger kinetic contribution for the ions.

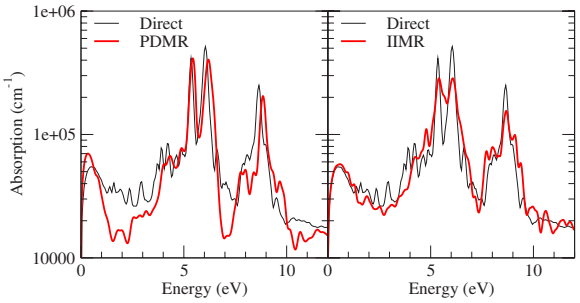

FIG. 9. (Color online) Computed absorption coefficient versus energy. (Left) PDMR (red thick line) and direct mixture computation (thin line). (Right) same with the IIMR.

F. Absorption spectra

By using formulas (3), (4), and (6) we deduced the absorption spectra from the optical conductivities. The absorption spectra for both mixing models are shown in Fig. 9. In black we show the spectrum obtained from the direct simulation of the mixture. The red-thick lines correspond to the spectra resulting from the composition of the pure phases obtained using the PDMR (left figure) or IIMR (right figure). It is clear from these results that the IIMR prediction from the absorption spectrum is closer to the direct computation than PDMR calculations. Once again, while the position in energy of the maxima are correct, their intensity appears underestimated when compared to the direct simulation results. The high values of the partial densities obtained in the PDMR model are clearly at the origin of this effect. It is not clear, however, how the mixture law can be modified to include this effect.

V. CONCLUSION

To summarize, we have presented experimental and simulation results for various aluminum and gold mixtures in the warm dense matter regime. Direct QMD simulations of the mixtures are in excellent agreement with experimental data both for the pressure and resistivities. Overall, we also have a good agreement for the pure elements equations of states and conductivities. Various mixing rules have been tested against full QMD simulations. We found that the predicted total pressures are in good agreement with the direct simulation results when using the PDMR. In contrast the resistivities of the mixture are underestimated when using this approach. The partial densities predicted with IIMR leads to improved resistivity results for the mixture when compared to the experiment. The optical conductivities and absorption coefficients obtained using this scheme are also in much better agreement with the result of the direct simulation of the mixture.

*jean.clerouin@cea.fr

[1] T. Guillot, Planet. Space Sci. **47** (1999).
[2] T. Guillot, W. B. Hubbard, D. J. Stevenson, and D. Saumon, *The Interior of Jupiter* (University of Arizona Press, Tucson, 2003).
[3] H. Iyetomi and S. Ichimaru, Phys. Rev. A **34**, 3203 (1986).
[4] S. Bastea, Phys. Rev. E **71**, 056405 (2005).
[5] R. L. Shepherd, D. R. Kania, and L. A. Jones, Phys. Rev. Lett. **61**, 1278 (1988).
[6] M. P. Desjarlais, J. D. Kress, and L. A. Collins, Phys. Rev. E **66**, 025401(R) (2002).
[7] P. Renaudin, C. Blancard, J. Clérouin, G. Faussurier, P. Noiret, and V. Recoules, Phys. Rev. Lett. **91**, 075002 (2003).
[8] G. Faussurier, C. Blancard, P. Renaudin, and P. L. Silvestrelli, Phys. Rev. B **73**, 075106 (2006).
[9] P. Renaudin, V. Recoules, P. Noiret, and J. Clérouin, Phys. Rev. E **73**, 056403 (2006).
[10] V. Recoules, P. Renaudin, J. Clérouin, P. Noiret, and G. Zérah, Phys. Rev. E **66**, 056412 (2002).
[11] D. A. Liberman, Phys. Rev. B **20**, 4981 (1979).
[12] G. Kresse and D. Joubert, Phys. Rev. B **59**, 1758 (1999).
[13] G. Kresse and J. Hafner, Phys. Rev. B **47**, R558 (1993).
[14] The choice between LDA and GGA was decided by computing equilibrium properties of solids in fcc phase. Moreover, we believe that at high temperature the effect of the exchange correlation approximation becomes less crucial.
[15] D. M. Ceperley and B. J. Alder, Phys. Rev. Lett. **45**, 566 (1980).
[16] S. Mazevet, M. P. Desjarlais, L. A. Collins, J. D. Kress, and N. H. Magee, Phys. Rev. E **71**, 016409 (2005).
[17] F. Hensel and W. W. Warren, Phys. Scr. **25**, 283 (1988).
[18] F. Hensel and W. W. Warren, *Fluid Metals* (Princeton University Press, Princeton, 1999).
[19] A. V. Bushman, I. V. Lomonosov, and V. E. Fortov, *Equation of State of Metals at High Energy Densities* (Institute of Chemical Physics, Russian Academy of Sciences, Chernogolovka, 1992) (in Russian).
[20] S. P. Lyon and J. D. Johnson, SESAME, The Los Alamos National Laboratory Equation of State Database, Report No. LA-UR-92–3407, 1992 (unpublished).
[21] R. M. More, K. H. Warren, D. A. Young, and G. B. Zimmerman, Phys. Fluids **31**, 3059 (1988).
[22] R. M. More, J. Quant. Spectrosc. Radiat. Transf. **27**, 345 (1982).
[23] R. Landauer, J. Appl. Phys. **23**, 779 (1952).